WAMAS: A Multi-Agent System with Improved Watershed Segmentation for Brain MRI Analysis

Nedjoua Houda Kholladi[1], Okba Kazar[2], Abdelkader Hima[3,4,*], Kamal Bechkoum[5], Mounir Beggas[6,7], Meriem Hamoud[6,7]

[1]University of Biskra, 07000 Biskra, Algeria
[2]College of Computing and Intelligent Systems, Department of Computer Science, University of Kalba, Sharjah, UAE
[3]University of El Oued, Fac. Technology, 39000 El Oued, Algeria
[4]University of El Oued, UDERZA Unit, Fac. Technology, 39000 El Oued, Algeria
[5]University of Gloucestershire, United Kingdom
[6]University of El Oued, Computer Science Department, LIAP, 39000 El Oued, Algeria
[7]University of El Oued, Informatics Department, Fac. Exact Sciences, 39000 El Oued, Algeria
E-mail: abdelkader-hima@univ-eloued.dz

Accurate segmentation of brain magnetic resonance imaging (MRI) scans is vital for early diagnosis and treatment planning of brain tumors. Classical methods such as the Watershed algorithm often suffer from over-segmentation, noise sensitivity, and limited adaptability. To address these issues, we propose a Watershed-based Multi-Agent System (WAMAS) that combines empirical thresholding, statistical similarity measures, and agent-driven negotiation for robust tumor delineation. In preprocessing, edge features are extracted with Canny and Sobel operators, while region descriptors are obtained via Quadtree decomposition and refined through mean–variance analysis to adapt thresholds under noise. During processing, Region Agents propose the proposed local watershed on its appropriate regions where seed candidate merges based on similarity scores, while Edge Agents validate boundaries using gradient consistency; conflicts are resolved through cooperative decision rules to prevent over-segmentation. Evaluations on BrainWeb and IBSR167 datasets under varying noise levels showed that WAMAS outperforms baseline Watershed and advanced methods such as U-Net and B-UNet, and best results obtained are respectively 97.38% accuracy, 96.50% sensitivity, and 96.84% specificity. Paired t-tests (p < 0.01) confirmed significant improvements. These results demonstrate that WAMAS provides coherent boundaries and robust performance, making it a promising tool for clinical neuroimaging.

Povzetek: Članek predlaga WAMAS, večagentsko različico metode zajezitve, ki z robnimi in regijskimi značilkami preprečuje prekomerno segmentacijo in zanesljivo izriše možganske tumorje.

1 Introduction

Brain image partitioning, commonly referred to as segmentation in medical imaging, aims at dividing MRI scans into disjoint regions corresponding to anatomical tissues or pathological structures [1, 2, 3]. Unlike semantic segmentation in natural images, brain MRI segmentation is concerned with delineating fine-grained structures such as white matter, gray matter, cerebrospinal fluid, and tumor subregions [4, 5]. Accurate partitioning of these regions is critical for downstream tasks including diagnosis, surgical planning, and radiotherapy guidance [6].

Traditional approaches relied on intensity thresholding [7], region growing [8], and watershed [9] transforms, which offered deterministic outcomes but struggled with intensity inhomogeneity and noise in MRI [10, 11]. The watershed transform, in particular, has been extensively employed for medical image partitioning due to its ability to extract precise boundaries [12, 13, 14]. However, its drawbacks over-segmentation and sensitivity to noise limit its standalone applicability in clinical pipelines [15, 16, 17].To mitigate this, watersheds have frequently been integrated as either preprocessing [18] or post-processing [19] modules in hybrid frameworks requiring high computational cost.

In recent years, deep learning has driven significant advances in brain MRI segmentation [20, 21, 22]. Convolutional neural networks (CNNs) and transformer-based models achieve state-of-the-art performance, yet they require large annotated datasets, exhibit poor generalization across scanners or institutions, and are computationally demanding [23, 24, 25, 26, 27]. This motivates research into model-driven alternatives that emphasize interpretability, efficiency, and robustness while maintaining competitive accuracy.

This paper introduces the Improved Watershed-basedMulti-Agent System (WAMAS), a cooperative framework that reformulates MRI segmentation as a negotiation process between region agents and edge agents. The pipeline proceeds as follows: (i) preprocess the MRI through noise reduction and contrast enhancement, (ii) extract candidate boundaries using multi-detector edge fusion, (iii) generate an over-segmented map via watershed, (iv) assign agents to both edges and regions, and (v) iteratively apply cooperation protocols: region–edge, edge–edge, and merging to produce agreement-based partitions. Figure 1 illustrates the output of this cooperative process on representative brain MRI slices.

The contributions of this work are fourfold: (i) a hybrid preprocessing and feature extraction scheme combining quadtree region decomposition and multi-scale edge fusion; (ii) an enhanced Watershed seeding strategy that leverages over-segmentation for controlled refinement; (iii) formalized cooperation and negotiation protocols between agents to balance edge precision and region homogeneity; and (iv) comprehensive evaluation of WAMAS on multiple MRI datasets, demonstrating improved robustness and generalization compared to both classical and learning-based baselines.

The remainder of this article is organized as follows. Section 2 reviews the related literature based watershed techniques, multi-agent systems, and recent state-of-the-art approaches based deep learning for brain MRI segmentation. Section 3 presents the WAMAS methodology, outlining its main steps: preprocessing, feature extraction, and MAS-based processing. Section 4 presents the experimental results, discussions, and comparisons. Lastly, Section 5 concludes the paper by discussing the main findings and outlining future perspectives.

2   Related work

The watershed transform, grounded in mathematical morphology, is a well-established segmentation method that interprets grayscale images as topographic surfaces, where bright pixels correspond to high elevations and dark pixels to low ones. Segmentation is performed by identifying catchment basins formed around regional minima, while watershed lines delineate the boundaries between them. When applied to gradient magnitude images, these lines align with areas of high intensity variation, thereby outlining object boundaries with precision [28, 29]. Owing to its simplicity and guarantee of complete image partitioning, the watershed method has been widely applied in medical imaging for tumor delineation and tissue boundary detection [30]. Nevertheless, its principal drawback lies in over-segmentation, particularly in noisy or low-contrast data. To mitigate this issue, researchers have proposed marker-based strategies [31], hybrid preprocessing pipelines [32], and the integration of anatomical priors [33], which collectively enhance the robustness and clinical applicability of watershed-based segmentation.

Watershed to morphological approaches, deep convolutional neural networks (CNNs) have achieved remarkable success in several medical image segmentation applications [34, 35, 36]. Recent models have advanced tumor boundary detection in MRI, yet persistent challenges remain. For example, Tiwary et al. [37] introduced an EfficientNet-enhanced UNet that demonstrated strong feature extraction capabilities, but its reliance on numerous parameters raises scalability concerns, especially for real-time or resource-constrained applications. Tejashwini et al. [38] proposed SLCA-UNet, which integrates spatial and local contextual attention to improve boundary delineation, yet its architectural complexity increases the risk of overfitting and limits generalization across datasets. Similarly, the FF-UNet framework [39] improved multi-scale feature fusion, but exhibited reduced robustness when applied to heterogeneous MRI modalities or highly imbalanced datasets. Taken together, these studies highlight that while CNN-driven methods achieve high segmentation accuracy, they continue to face critical issues such as computational burden, sensitivity to heterogeneity, and limited cross-dataset adaptability [40]. A comparative overview of these limitations is summarized in Table 1.

To overcome these challenges, recent works have explored intelligent multi-agent systems (MAS) as adaptive and context-aware solutions. Unlike CNNs, which operate within rigid architectures, MAS frameworks allow agents to collaborate and negotiate in order to extract the most relevant features and refine segmentation outcomes dynamically. For instance, Allioui et al. [44] developed a multi-agent environment for automated Alzheimer's diagnosis, showing how coordinated agents can effectively capture discriminative brain imaging features. Bennai et al. [45] introduced a stochastic multi-agent approach for brain tumor segmentation, demonstrating robustness against variability in MRI data. Beyond medical imaging, Xia et al. [46] employed multi-agent reinforcement learning to optimize UAV swarm tracking, illustrating the versatility of agent-based decision-making in complex environments. These contributions underscore the potential of combining watershed-based segmentation with MAS, leveraging the interpretability and coverage of watershed while mitigating over-segmentation through intelligent, adaptive feature selection.

3   Proposed approach

Medical image processing, particularly segmentation, faces challenges in data acquisition, sophisticated modeling, and efficient information dissemination. Multi-Agent Systems offer a promising solution by enabling distributed control, collaborative problem-solving, and conflict resolution [47, 48, 49], despite potential limitations in autonomous agent expertise.

The WAtershed-based Multi-Agent System is a de-

Table 1: Summary of selected research works on brain tumor segmentation

Research paper	Model	Dataset	Key Contributions	Metric Score	Advantage	Inconvenient
Saifullah et al. (2025) [41]	Preprocessing: CLAHE & HE; Processing: Modified U-Net + Attention Gate	BraIS 2021	Attention Gating: Salient region; Histogram Equalization: reduce low intensities; combination for irregular geometries	Dice: T1E: 0.9521 T1: 0.9093 T2: 0.9216 Flair: 0.8556	Good segmentation performance; robust across modalities; enhanced accuracy	High computational cost; limited external generalizability
Ho et al. (2025) [42]	Mask R-CNN + transfer-learned DeepMeslic	139 T2-weighted scans	Automated segmentation; volumetric quantification of radiation-induced changes	Average Dice = 71.8%	Supports clinical decision-making; approximates manual volumetric segmentation	Lower accuracy; Small Dataset; task-specific
Angona & Mondal (2025) [43]	3D ResAttU-Net-Swin hybrid model	BraIS 2020 & 2019 datasets	Novel fusion of residual U-Net, attention skip-connections, and Swin Transformer	BraIS 2020: DSC = 88.27%, IoU = 79.93%; BraIS 2019: DSC = 89.20%, IoU = 81.40%	Balanced performance; powerful context modeling; multi-scale feature learning	Slightly lower DSC; complexity increases training cost

centralized framework designed for precise and statistically consistent medical image segmentation. It uses autonomous region, sub-region, and edge agents that cooperate through communication and negotiation. Sub-region agents apply watershed transformations, region agents manage dynamic merging, and edge agents validate boundary connections. Decision-making incorporates local Watershed variance-based measures, homogeneity predicates, and Ward's cost, while communication uses finite-state machine modeling for conflict resolution and adaptive coordination. WAMAS integrates distributed control, collaboration, and adaptability for robust, scalable, and high-accuracy segmentation.

The WAMAS framework combines classical image processing with intelligent agent-based decision-making. It involves preprocessing for image quality enhancement, feature extraction for reliable maps, and a cooperative MAS for robust segmentation (see Figure 1).

3.1 Preprocessing

The preprocessing phase is crucial for brain MRI segmentation, enhancing image quality, suppressing noise, and improving visibility of diagnostically relevant features. Brain MRI often suffers from noise and low contrast. Noise reduction uses median and Rician filters, while contrast is enhanced via histogram equalization. These steps ensure cleaner, sharper images for precise edge detection and region segmentation (see Algorithm 1).

Algorithm 1: Brain MRI Image Preprocessing for Noise Reduction and Contrast Enhancement

---

Input: Raw MRI image $I_{\text{raw}}(x, y)$ of size $M \times N$

Output: Preprocessed enhanced image $I_{\text{Enhanced}}(x, y)$

Parameters: Kernel size k for median filter; Rician noise suppression operator $\mathcal{R}(\cdot)$; Histogram equalization function $T(\cdot)$;

Step I: Salt-and-Pepper Noise Reduction;
$$I_{\text{med}}(x, y) := \underset{(s,t) \in \Omega_{k \times k}}{\text{median}} \{I_{\text{raw}}(x + s, y + t)\};$$

Step II: Rician Noise Suppression;
$$I_{\text{rician}}(x, y) := \mathcal{R}(I_{\text{med}}(x, y));$$

Step III: Contrast Enhancement;
$$I_{\text{Enhanced}}(x, y) := T(I_{\text{rician}}(x, y));$$

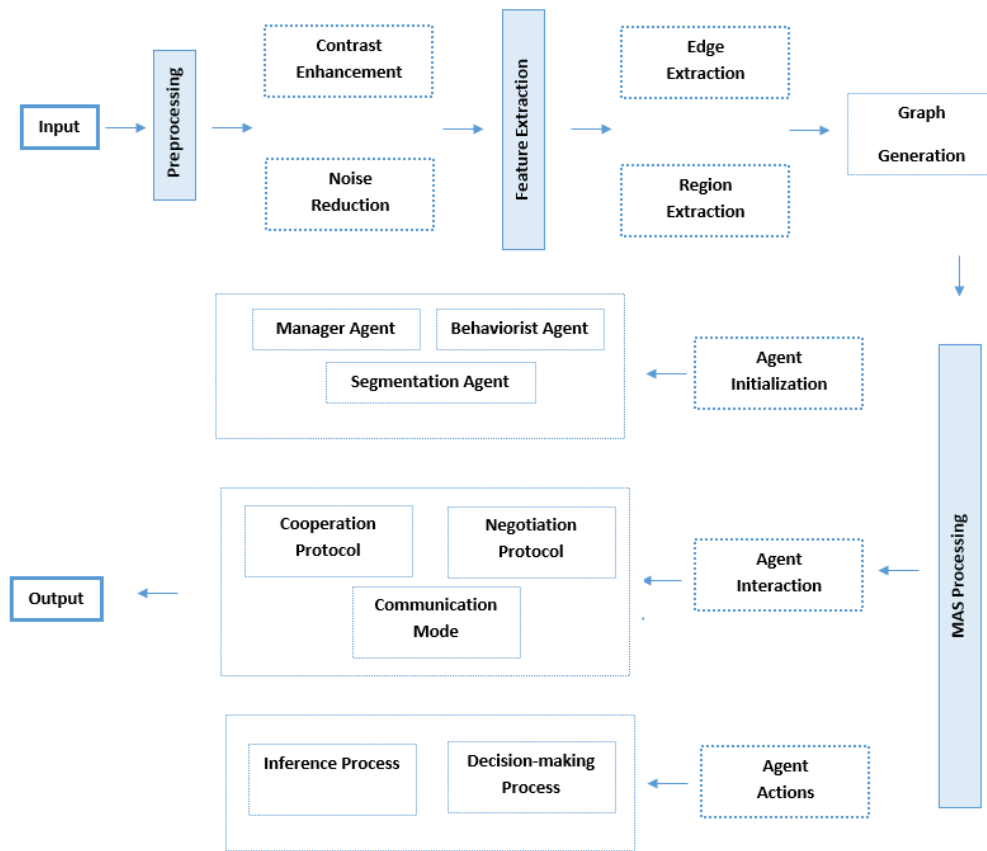**return** I_{Enhanced};

Figure 1: Flowchart of the proposed watershed-based multi-agent system framework for brain image segmentation framework: (WAMAS).

3.2 Feature extraction, feature map identification and graph generation

The feature detection and hierarchical graph generation pipeline initiates with a multi-method edge estimation strategy to ensure comprehensive feature capture. A robust feature extraction is performed to generate edge from six edge detectors. In the other hand, region detection based Quadtree algorithm is applied to extract region map. These maps represent the primary objects of interest for agent assignment in later phases.

3.2.1 Edge feature extraction

Edge detection identifies significant boundaries between different tissue regions. Since no single operator is universally reliable, multiple classical edge detectors as Robert, Prewitt, Deriche, Shen-Castan, Canny, and Laplacian of Gaussian (LoG) are integrated.

a) Edge Core Detection

First-order gradient-based edges are computed by convolving the input image with Sobel/Prewitt operators to obtain horizontal (G_x) and vertical (G_y) gradients, from which the magnitude $G(x,y) = \sqrt{G_x^2 + G_y^2}$ is derived.

This is supplemented by second-order derivative detection through the Laplacian of Gaussian (LoG), calculated as $LoG(x,y) = \nabla^2(G_\sigma(x,y) * I(x,y))$ to enhance edge localization at a specific scale. The optimal parameter set for an edge detector ϵi is determined by maximizing a weighted correlation criterion that integrates intensity-based correlation, joint entropy, and distribution alignment with a reference edge map G. Formally: $j^* = \arg\max_j [\alpha \operatorname{Corr}(O_{ij}, G) + \beta \operatorname{Corr}_1(O_{ij}, G) + \gamma \operatorname{Corr}_2(O_{ij}, G)]$ where O_{ij}^e and $\alpha + \beta + \gamma = 1$; ensuring robust parameter optimization across statistical, information-theoretic, and distributional measures. Furthermore, textural cues are incorporated by computing a 14-dimensional Haralick feature vector from the image's Gray-Level Co-occurrence Matrix (GLCM), with salient features like contrast f_2, entropy f_9, and homogeneity f_5, being leveraged to derive a supplementary edge strength measure.

b) Optimal Edge Map Agglomeration

The resultant edge ϵi responses are consolidated, refined via non-maximum suppression and hysteresis thresholding to produce a thin, connected binary edge map, and subsequently processed by a contour tracing algorithm to extract a preliminary set of closed contours. These contours undergo morphological post-processing using dila-

tion $A \oplus B = \{z \mid (\hat{B})_z \cap A \neq \emptyset\}$ to bridge gaps and erosion $A \ominus B = \{z \mid B_z \subseteq A\}$ to remove noise; followed by an optimization step to eliminate redundant contours $O_{ij}^e(I_n, \varepsilon_i)$ based on geometric properties.

The optimized contours are rendered into a final binary edge map M_{ij}^e.(See algorithm 2)

Algorithm 2: Edge Feature Detection:Edge-Map-Prepro Generation

---

Input: Input image $I_E nhanced$, set of edge
        detectors $\mathcal{E} = \{\epsilon_1, \epsilon_2, ..., \epsilon_6\}$
Output: Consolidated binary edge preprocessing
        map, Edge-Map-Prepro
forall $\epsilon_i \in \mathcal{E}$ // Step I: Optimize
 parameters per detector **do**
    | $j^* \coloneqq {}_j O(I_E nhanced, \epsilon_i, P_{ij})$;
    | $O_i^e \coloneqq \epsilon_i(I_E nhanced, P_{ij^*})$;

forall *pixel positions* **x**   // Step II: Fuse
 optimal detector outputs **do**
    | $M^e(\mathbf{x}) \coloneqq \bigvee_{i=1}^6 O_i^e(\mathbf{x})$;

repeat
    forall x do
        | $M_{\text{dil}}(\mathbf{x}) \coloneqq \bigvee_{\mathbf{y} \in N(\mathbf{x})} M^e(\mathbf{y})$;
        | // Dilation
    $M^e \coloneqq M_{\text{dil}}$;
    forall x do
        | $M_{\text{ero}}(\mathbf{x}) \coloneqq \bigwedge_{\mathbf{y} \in N(\mathbf{x})} M^e(\mathbf{y})$;
        | // Erosion
    $M^e \coloneqq M_{\text{ero}}$;
until *morphological operation cycle complete*
 // Step III: Morphological
 post-processing;
Edge-Map-Prepro $\coloneqq M^e$;

3.2.2 Region feature extraction

Region features are extracted via tessellation, partitioning the image based on homogeneity. The Quadtree decomposition method is used for hierarchical region representation within Regions of Interest (Algorithm 3).

3.2.3 Feature map identification and graph generation

Following the extraction of the optimized edge map $E_optimal$ and the set of homogeneous regions $\mathcal{H}$ from the Quadtree segmentation, the image structure is represented through three distinct graph formulations. This map encodes spatial relationships and is subsequently used by agents to establish adjacency and nearest-neighbor graphs (see algorithm 4).

Algorithm 3: Quadtree-Based Hierarchical Region Variance

An input image I, a homogeneity threshold τ, a minimum region size $s_{\min}$ A set of homogeneous regions $\mathcal{H}$, a quadtree segmentation map Q_{map}

Initialization: Define entire image as initial region
 R_0
Initialize empty set $\mathcal{H}$
Initialize queue $\mathcal{Q}$
$\mathcal{Q}.\text{push}(R_0)$

while $\mathcal{Q}$ *is not empty* **do**
    Process all regions in the queue $R \coloneqq \mathcal{Q}.\text{pop}()$
    if $size(R) \leq s_{min}$ **then**
        | Termination condition met $\mathcal{H} \coloneqq \mathcal{H} \cup R$
        | $Q_{\text{map}}(R) \coloneqq 0$
        | **continue**
    else
        | $\sigma_R^2 \coloneqq \text{Variance}(R)$
        | **if** $\sigma_R^2 < \tau$ **then**
            | Region is homogeneous $\mathcal{H} \coloneqq \mathcal{H} \cup R$
            | $Q_{\text{map}}(R) \coloneqq 0$
        | **else**
            | Region is heterogeneous; split
            | $Q_{\text{map}}(R) \coloneqq 1$
            | Partition R into four quadrants:
                $Q_1 = I(x : x + \frac{w}{2}, \ y : y + \frac{h}{2})$
                $Q_2 = I(x + \frac{w}{2} : x + w, \ y : y + \frac{h}{2})$
                $Q_3 = I(x : x + \frac{w}{2}, \ y + \frac{h}{2} : y + h)$
                $Q_4 = I(x + \frac{w}{2} : x + w, \ y + \frac{h}{2} : y + h)$
            forall $Q_k \in \{Q_1, Q_2, Q_3, Q_4\}$ **do**
                | $\mathcal{Q}.\text{push}(Q_k)$

return $\mathcal{H}$, Region-Map-PreproQ_{map}

3.3 MAS processing

The WAMAS framework systematically addresses challenges in feature identification, noise removal, and information extraction through sophisticated cooperation protocols. The System Manager configures agent activities, deploys segmentation agents, and aggregates results. Agents navigate conflicting, growing, complex situations, and priority decision-making while pursuing a common goal.

3.3.1 Agent initialization

The system manager configures agent status, supervises placement of segmentation and behaviorist agents on image slices, and aggregates results. Agent interactions are categorized into conflicting, growing, or complex scenarios for effective management.

a) Manager Agent (Implicit Control)

The manager agent is central to WAMAS, configuring status, supervising activities, and overseeing segmentation. It initializes agents, positions them strategically, and aggregates results.

Algorithm 4: Graph Construction from Features Maps

Input : Optimized edge map $E_{optimal}$, set of homogeneous regions $\mathcal{H} = \{R_1, R_2, ..., R_n\}$, number of neighbors k

Output: Region-Edge Graph G_{RE}, Region Adjacency Graph G_{RAG}, Nearest-Neighbor Graph G_{NN}

Initialization:

$V \leftarrow \{v_i \mid v_i \text{ corresponds to region } R_i \in \mathcal{H}\}$

$c_i \leftarrow \text{centroid}(R_i) \quad \forall R_i \in \mathcal{H}$

$\mu(R_i) \leftarrow \text{mean feature vector of } R_i$

forall *region pairs* (R_i, R_j) *where* $i < j$ **do**
    if $R_i \cap Dilate(R_j) \cap E_{optimal} \neq \emptyset$ **then**
       $E_{RE} \leftarrow E_{RE} \cup \{e_{ij}\}$;   // Build Region-Edge Graph G_{RE}

foreach $e_{ij} \in E_{RE}$ **do**
    $w_{ij} \leftarrow \|\mu(R_i) - \mu(R_j)\|_2$; // Build G_{RAG} with weights

foreach $R_i \in \mathcal{H}$ **do**
    $\mathcal{N}_k(i) \leftarrow \{j \mid$
    $d(c_i, c_j)$ is among k smallest values$, j \neq i\}$
    foreach $j \in \mathcal{N}_k(i)$ **do**
       $E_{NN} \leftarrow E_{NN} \cup \{(v_i, v_j)\}$;   // Build G_{NN} Graph

$G_{RE} \leftarrow (V, E_{RE})$
$G_{RAG} \leftarrow (V, E_{RE}, W)$ where
$W = \{w_{ij} \mid e_{ij} \in E_{RE}\}$
$G_{NN} \leftarrow (V, E_{NN})$
return G_{RE}, G_{RAG}, G_{NN}

The lifecycle of the manager-controlled agents follows five key steps.

Step 1 : Agent Initialization: After preprocessing, the manager processes region and edge maps, assigning corresponding tasks to agents.

Step 2 : Agent Self-Reproduction: Upon detecting a feature pixel p, an agent generates offspring agents in nearby regions or in random orientations, thereby enhancing feature extraction. Agent selection is guided by:

$$F(A_i) = \begin{cases} 1 - \dfrac{\text{N steps before self-reproduction}}{\text{Life-span of } A_i}, \\ \text{if condition holds,} \\ -1, \text{otherwise.} \end{cases}$$

It quantifies the time it takes for the agent to locate a feature pixel. Updating Direction Vectors: for each selected agent, it calculates the following equation:

$$DV(\theta \in \Theta)_\theta = \frac{N_\theta}{\sum_{\forall i} N_i} \ \wedge \ DV(\omega \in' \Omega) = \frac{O_\omega}{\sum_{\forall i} O_i}$$

Where θ, ω: directions, Θ: Lattice of agent's directions, $'\Omega$: Grid Lattice of agent's directions, O_i: Orientation.

Step 3 : Agent Modification: Agents update structural parameters (e.g., edge length, intensity, grayscale values) when protocols such as edge extension alter segmentation boundaries.

Step 4 : Agent Scheduling: Similar to an operating system scheduler, agents prioritize actions through finite automata states, ensuring sequential execution of tasks.

Step 5 : Agent Termination: Agents have finite lifespans and vanish once exceeded, with only the surviving agent persisting in competitive edge-connection scenarios. At the end state, agents mark themselves inactive while monitoring the resulting edge map, ensuring that system convergence is achieved.

b) Behaviorist Agent

A recent research direction explores autonomous agent systems for studying emergent behaviors within a lattice. Agents interact with digital image environments according to predefined behavioral rules, exhibiting activities such as self-reproduction and both randomized and deterministic search strategies. Central to this approach is the "Based Local Stimulus", which defines the distribution density:

$D^\kappa_{I(i,j)} = \sum_{s=-\kappa}^{\kappa} \sum_{t=-\kappa}^{\kappa} \{1 \mid \|I(i+s, j+t) - I(i,j)\| < \delta\}$ Where: κ a radius around the agent's neighboring regions, i.e., a circle centered on that agent at $(i; j)$; $s; t$: an index identifies a pixel in a neighboring' concerned region (i, j); $I(i; j)$: the value of grey level $(i; j)$; δ: A predetermined positive threshold. During execution, one agent exits the system, while the manager agent is responsible for enforcing the survival criterion remained. This agent integrates all essential information required for segmentation, summarized in Table S1.

b) Segmentation Agent

Segmentation agent act as 'Supervisor Agent' in detecting optimal features of interest, collecting criteria specific to their type either region agents or edge agents. (attributes in Table S1) Also, it initializes two categories of agents: edge agents, responsible for detecting contours, and region agents, focused on identifying homogeneous areas that support boundary exploration. Both types share statistical and geometrical features, with pixels $P(x, y)$ derived from an image $I(x, y)$ of size $N \times N$ denoting the number of distinct grey levels. These features include grey-level intensity $\rho(i, j)$ and correlation coefficients, which capture relationships between neighboring pixels. Within the cooperative WAMAS framework, segmentation agents collaboratively manage contour and region results (Figure 2). Also, segmentation agent acts as Supervisor Agent in detecting optimal features of interest, collecting criteria specific to their type either Region Agents or Edge Agents.

The segmentation agent supervises (i) The proposed merging process is carried out through a local watershed-based variance algorithm, effectively operating on sub-regions, (ii) MAS-based cooperation protocols , (iii) negotiate priorities between edge and region agents to resolve conflicts, (iv) use inference rules to determine optimal in-

teractions, and (v) apply decision-making for either best merging or partitioning.

– Edge Agent: Assigned to edges from the edge map. Its attributes include statistical and geometrical features of its assigned edge (e.g., length, gradient mean/direction, pixel list).

– Region Agent: Assigned to homogeneous regions from the region map. Its attributes include grayscale values, a list of edge identifiers, and sub-region data. Each region apply a novel local watershed-based variance (see Algorithm 5). Its core functions are:

Algorithm 5: Proposed Variance-Based Watershed Segmentation on Preprocessed Regions

---

Input: Preprocessed regions $\{R_i\}_{i=1}^n$ from Region-prepro-map, where $n = 255$
Output: Segmented image S
Initialization:;
Set empirical threshold: Emp-THR = 0.5;
Extract edge map E from region boundaries in $\{R_i\}$ using RAG and NNGSR$_i$;
foreach *region* $R_i \in \{R_i\}_{i=1}^n$ // Main processing loop **do**

   Step 1: Watershed Seed Selection via Regional Variance Analysis;
   // Compute regional variance metrics
   $\sigma^2(R_i) := \sum_{j=1}^m P(SR_j) \cdot \sigma^2_{SR_j}$;
   $\sigma^2(R_i) := \sum_{j=1}^m P(SR_j) \cdot (\mu_{SR_j} - \mu_{R_i})^2$;
   $\sigma^2_{\text{total}}(R_i) := \sigma^2(R_i) + \sigma^2(R_i)$;
   // Seed point selection
   foreach *sub-region* $SR_j \in R_i$ **do**
     if E_i *surrounds* SR_j *and*
     Emp-THR $\geq \sigma^2(R_i)$ **then**
       Mark SR_j surrounding E_i as seed point;

   Step 2: Regional Watershed Transformation via Flooding Simulation;
   $h_{\min}(R_i) := \min_{p \in R_i} I(p)$;
   $h_{\max}(R_i) := \max_{p \in R_i} I(p)$;
   for $h := h_{\min}(R_i)$ **to** $h_{\max}(R_i)$ // Intensity levels iteration **do**
     $X_h(R_i) := \{p \in R_i \mid I(p) \leq h\}$;
   $\text{Watershed}(R_i) := \bigcup_h \partial(X_h(R_i))$;
   // Boundary union
   Step 3: Region-Specific Segmentation;
   $S_{R_i} := \text{Watershed}(R_i) \cup \{\text{selected seed points}\}$;
Final Integration:;
$S := \bigcup_{i=1}^n S_{R_i}$ // Combine all processed regions

---

a. Local Watershed Initialization: Applies the Watershed algorithm to its region to generate an initial over-segmentation into sub-regions.

b. Proposed Watershed-based Variance: Manages subregions and computes merging predicates based on statistical variance and spatial metrics.

c. Dynamic Merging Style: Executes an iterative, predicate-based merging process of adjacent sub-regions.

3.3.2   Agent interaction

The Multi-Agent System (MAS) relies on reaction-driven interactions to achieve optimal control for precise segmentation. Cooperation protocol implements key constraints: edge-to-edge, edge-to-region, and region-to-sub-region, to structure these interactions. Together, these algorithms define agent mapping strategies and their relational mappings within the MAS framework. Interactions are further regulated by negotiation protocols and communication modeled as a Finite-State Machine (FSM), ensuring adaptive and consistent decision-making.

a) Cooperation Protocols

This protocol establishes a mutual agreement to connect two adjacent edges. The connection is determined by computing the correlation between regions and edges using their respective mean (μ)and variance (σ). A dynamic threshold is calculated for each region, and each edge E_i is assigned a weight $W(E_i)$

Protocol1: Edge-Edge Cooperation for Region Meditation :

In the proposed framework, edge–edge cooperation protocol relies on statistical texture attributes extracted from the gray-level co-occurrence matrix (GLCM) combined with geometric descriptors. Each edge agent computes a normalized feature vector: $F_k = [f^{(\mu)}, f^{(\sigma)}, f^{(Energy)}, f^{(Corr)}, f^{(SumAvg)}, f^{(Entropy)}, f^{(\theta)}]$ where entropy-based terms H_{XY}, H_{XY1}, H_{XY2} reflect randomness, while θ encodes edge orientation (see Table S2). Cooperation between two edges E_k and E_l is governed by a weighted difference score μ_k and μ_l with $\mu_k = \sum_a w_a \left| f_k^{(a)} - f_R^{(a)} \right|$, $\mu_l = \sum_a w_a \left| f_l^{(a)} - f_R^{(a)} \right|$, where $f_R^{(a)}$ represents the reference region attributes and w_a are normalized weights.

If $\mu_k \leq$ THR and $\mu_l \leq$ THR the geometric consistency conditions $\Delta L_{\text{rel}} = \frac{|L_k - L_l|}{\max(L_k, L_l)} < \tau_{\text{len}}$, $|\theta_k - \theta_l| < \tau_\theta$ are satisfied, then the Region Adjacency Graph (RAG) is updated as New_RAG $\leftarrow$ ConnectRegion(E_k, E_l). This attribute-aware cooperation ensures that only edges with statistically coherent profiles and structural alignment are merged, thereby improving the robustness of the segmentation process and preventing spurious over-merging in heterogeneous image regions.

Protocol2: Edge-Region Cooperation : Uses adjacency maps to extend boundaries.

Edge-to-Region Protocol for Boundary Extension: This protocol employs adjacency maps to extend regional boundaries through edge cooperation. For each region $R_i \in \mathcal{R}$ a region–edge graph is constructed as $G_{(R_i, E)} = (R_i, \{E_k\}_{k=1}^m)$, where each E_k denotes an adjacent edge. For any pair of edges $\langle E_k, E_l \rangle \in G_{(R_i, E)}$ with $k \neq l$
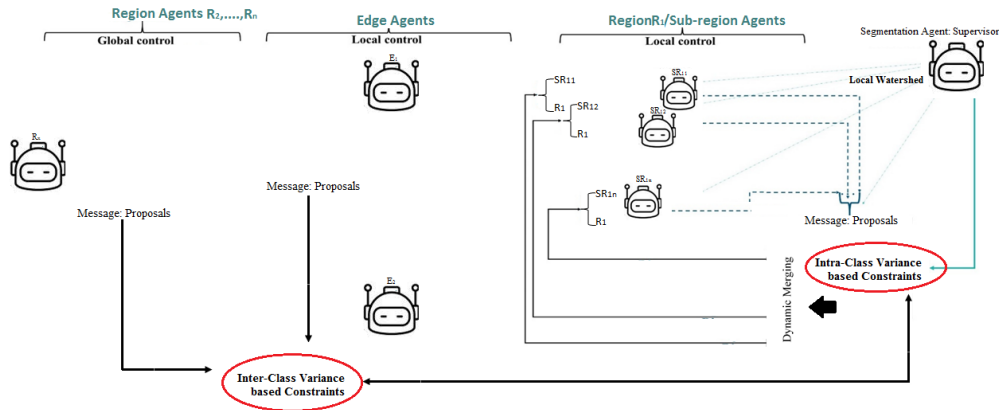
Figure 2: Proposed Of local watershed-based variance and hierarchy agent architecture

the Euclidean distance between their centroids is defined as $D(E_k, E_l) = \|C(E_k) - C(E_l)\|_2$ denotes the centroid of the Edge E_k.

If the weight difference between two edges satisfies: $|W(E_k) - W(E_l)| < \mathrm{THR}_R$ and $D(E_k, E_l) = \min_{p \neq q} D(E_p, E_q)$ then the Region Adjacency Graph is updated as New_RAG $\leftarrow$ MergeEdges(E_k, E_l) Alternatively, if $W(E_k) = W(E_l) \wedge D(E_k, E_l) \leq \mathrm{Dist}_{\mathrm{THR}}$, the edges are extended according to Execute_Extension(E_k, E_l), subject to Survival_Criterion(E_k, E_l). This protocol ensures that boundary extension is driven by both statistical similarity $W(E_k)$ and spatial proximity $D(E_k, E_l)$, while maintaining structural consistency through survival criteria.

Protocol 3: Edge-Checking Based Sub-Region Merging

For every pair of edges E_k, E_l in E_i with $k \neq 1$, the sub-region merging process is initiated: (SR_i, SR_j) extracted from (R_i, R_j). The distance between their corresponding agents is defined as:

$$\mathrm{Dist}\left(\mathrm{Ag}^{R_i}_{SR_i} : SR_i, \; \mathrm{Ag}^{R_j}_{SR_j} : SR_j\right) = \frac{\mu_{SR_i} + \mu_{SR_j}}{2}$$

where μ_{SR_i} and μ_{SR_j} represent the mean attributes of the respective sub-regions. If $\mathrm{Dist}(SR_i, SR_j) \wedge \mathrm{Adjacent}(SR_i, SR_j, RAG)$ then the merge operation is executed: Merge(SR_i, SR_j), Update$\big(RAG, RAG_{SR_i}, G_{(R_i, E)}, NNG_{(SR_i, E)}\big)$. This ensures that merging occurs only between statistically similar and topologically adjacent sub-regions.

Protocol4: Region to Sub-region Dynamic Merging Process:

This protocol guides merging operations based on watershed initialization, leveraging both edge attributes and region-agent descriptors. Morphological operator $(\ominus, \oplus)$ and distance transforms dist_transform > 0 are applied for the proposed Watershed. Threshold values are constrained within the interval $0.5 < \mathrm{Threshold} < 1.5$. While markers, border types, and border values are encoded as symbolic

or numeric labels. The hydrological analogy of watershed geometry is used to regulate merging(Watershed Fig). The average watershed altitude is defined in the (See Table S3)

Checking process:

if $\Delta = \big|\mathrm{Luminance}(SR_i) - \mathrm{Luminance}(SR_j)\big|$

If $\Delta < \mathrm{THR}$, then: $\begin{cases} H_a(SR_i) - H_a(SR_j) < \varepsilon_H \\ H_m(SR_i) - H_m(SR_j) < \varepsilon_M \\ S_a(SR_i) - S_a(SR_j) < \varepsilon_S \end{cases}$

then Send_Proposal(SR_i, SR_j)

If Mutuel_Proposal(SR_i, SR_j) then:

$$\begin{cases} \mathrm{New\_RAG} \leftarrow \mathrm{MergeSubRegion}(SR_i, SR_j) \\ \mathrm{Update\_Graphs}(RAG, RAG_{SR_i}, \\ G_{(R_i, E)}, NNG_{(SR_i, E)}) \end{cases}$$

b) Negotiation Protocols

The negotiation mechanism extends Ward's minimum variance criterion to govern interactions between region and edge agents, ensuring statistically optimal merging while preserving boundaries. Two complementary formulations are employed: a standard Ward's criterion for (region/sub-region) merging, and a generalized Ward's constraint that emphasizes edge preservation by penalizing large intensity discontinuities.

Ward's Criterion for Agent Negotiation

- Standard Ward's (for Region and sub-region Merging):

$$w^W_{ij} = \left[\frac{|R_i| \cdot |R_j|}{|R_i| + |R_j|}(\mu_i - \mu_j)\right]^2$$

(where $|R_i|$:Pixel count in region, μ_i: mean intensity of a given region R_i.)

- Edge-Region Conflict Resolution based Generalized Ward's constraint:

$$w_{ij}^G = \left[\frac{|R_i| \cdot |R_j|}{|R_i| + |R_j|} (\mu_i - \mu_j) \right]^4$$

constraint penalizes enormous intensity changes more antagonistically which is appropriate for edge preservation.

Protocol 1: Edge-Region Boundary Mediation

Once an edge E_i agent crosses region R_i boundary $\mathcal{B}_i$

Step1: Perceptual Data Acquisition

- Each Edge agent calculates edge strength:

$E_k = \frac{1}{|\mathcal{P}|} \sum_{p \in \mathcal{P}} \|\nabla I(p)\|, \quad \mathcal{P} = $ edge pixels near $\mathcal{B}_i$

- Each Region agent calculates the constraint Ward's cost of shifting $\mathcal{B}_i$: $w_{ij}^G = \left[\frac{|R_i| \cdot |R_j|}{|R_i| + |R_j|} \|\mu_i - \mu_j\| \right]^4$, for neighboring regions R_i and R_j

Step2: Decision Rule

- Adjust boundary:

if $\frac{E_k}{w_{ij}^G} > \tau_E$, with $\tau_E = 0.5$ (empirically tuned).

- Analysis: High-gradient edges replace boundary delineations only under the constraint of a low Ward cost value.

Protocol 2: Region Merging Process based Edge Authentication

Let two regions R_i, R_j propose merging

Step1: Ward's Merge Constraint

$$w_{ij}^W = \left[\frac{|R_i| \cdot |R_j|}{|R_i| + |R_j|} \|\mu_i - \mu_j\| \right]^2$$

Step2: Edge Mutual Agreement Authentication ($\mathcal{M}_{AA}$) Initiate queries to edge agents E_k located along the boundary $\mathcal{B}_i \cap \mathcal{B}_j$:

$$M_{AA} = \frac{1}{N} \sum_{k=1}^{n} I\left(\|\nabla I(p_k)\| < \tau_{\text{weak}} \right)$$

Step3: Merge Condition

$\left(w_{ij}^W < \tau_W \right) \wedge (M_{AA} > 0.7)$

Knowing that τ_W is dynamic threshold determination used for image-scale based Ward's cost distribution.

b) Agent Communication Mode based Finite State Machine Communication among agents is mediated through message exchange (Figure 3a), comprising two categories. "Proposal messages" are initiated by a manager agent to establish negotiation with peers. Upon receipt, the target agent computes a distance metric to evaluate feasibility, reflecting a unidirectional desire to cooperate. In contrast, "Order messages" are binding, either confirming mutual intent or enforcing constraints in decision-making. These are executed immediately (Figure 3b)

(a) agents communication mode
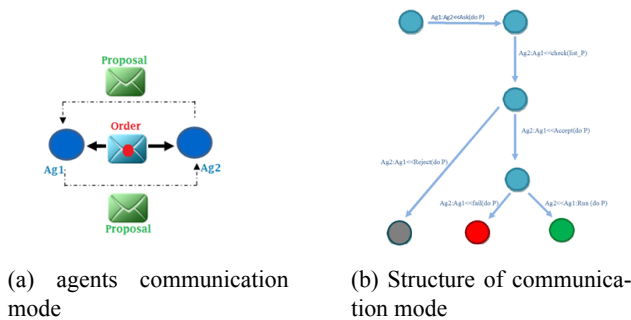
(b) Structure of communication mode

Figure 3: Agent communication mode

Agent behavior is formalized using a "Finite-State Machine (FSM)" (Figure 4), offering two advantages: (i) it

provides a global view of agent activities, and (ii) states and transitions are explicitly defined, enabling straightforward modifications.
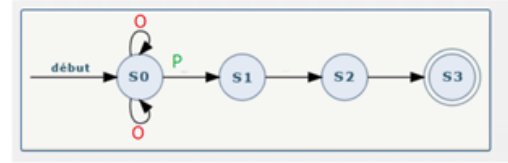

Figure 4: Finite-state machine functioning

The FSM governing edge connections and sub-region merging comprises four states:

State S0: Estimation of Closest Object of Interest: Edge agents compute distances to neighbors, dispatching propositions. Region agents evaluate sub-regions for merging based on homogeneity, continuity, and similarity, constructing graphs and applying merging predicates.

State S1: Reading and Analyzing Messages: Messages are processed. Orders are executed immediately, returning to S0. Proposals lead to S2.

State S2: Execution of Concerned Operation: Agents execute proposed actions (connecting edges, merging regions, splitting, extending contours) based on similarity, gradient direction, and contour weight. A "Survival Criterion" removes the weaker of competing agents.

State S3: Termination and Update: The manager agent finalizes execution, transitioning agents to a passive state and updating system graphs.

3.3.3 Agent actions

Agents optimize segmentation by selecting merge/extend actions A_{ij} that maximize region similarity and edge alignment while minimizing Ward's cost. Region agents contribute similarity and distance measures, edge agents provide alignment cues, and the agent manager enforces adjacency and order constraints.

a) Inference Process

The inference process is formulated as an optimal control problem in a cooperative multi-agent system with stochastic dynamics. Agents collaborate to achieve target states through coordinated tasks while preserving system stability. The dynamics assume full controllability and observability, with autonomous actions distributed across agents and complete access to the global state. The objectives are twofold: (i) "maximize inter-region task accumulation", such as merging statistically similar sub-regions, and (ii) "minimize intra-region conflicts", including erroneous edge extensions. These objectives are realized through a combination of instantaneous fusion and joint sub-region fusion or edge extension, reflecting the collective goals of the agents.

The merge selection action is formalize as an agent-aware optimization over candidate adjacent sub-region pairs SR_{ij} in the Region Adjacency Graph (RAG). Introduce binary decisions $m_{ij} \in \{0, 1\}$ (1 = merge) and define

region similarity $RS_{ij} = \exp\left(-\frac{\|f(R_i)-f(R_j)\|_2}{\sigma_f}\right)$, centroid distance $D_{ij} = \|C_i - C_j\|_2$, statistical contrast $\Delta_{ij} = |\mu_i - \mu_j|$, adjacency predicate to merge $APM_{ij} \in \{0,1\}$ and edge-alignment $EA_{ij} \in \{0,1\}$ (edge agents compute EA_{ij} as the mean dot product of unit gradients along the shared boundary weighted by normalized gradient magnitudes).

We maximize total merge utility $\max_{m_{ij}\in\{0,1\}} \sum_{i,j} m_{ij} U_{ij}$, $U_{ij} = \alpha\frac{RS_{ij}}{1+\Delta_{ij}} + \beta\frac{1}{1+D_{ij}} + \gamma EA_{ij}$, subject to agent and manager constraints: $m_{ij} \leq APM_{ij}$ (adjacency required), $m_{ij} \leq 1\{RS_{ij} \geq \rho_{\min}\}$, $m_{ij} \leq 1\{\Delta_{ij} \leq \Delta_{\max}\}$, $m_{ij} \leq 1\{EA_{ij} \geq \eta\}$, $\sum_{j:(i,j)\in RAG} m_{ij} \leq 1$, (no conflicting multi-merge), and $\text{Order}_{ij} = 1 \implies m_{ij} = 1$, (manager override). Practical MRI starting values (normalize intensities/features to [0,1]) are $\rho_{\min} = 0.80$, $\eta = 0.70$, $d_0 = 5$–15 pixels (or 1.0–3.0 mm), $\Delta_{\max} = 0.08$–0.12, $\sigma_f = 0.1$–0.2; recommended weights are $(\alpha,\beta,\gamma) = (0.45, 0.25, 0.30)$.

This formulation explicitly assigns region agents the role of proposing merges via RS_{ij}, δ_{ij}, and D_{ij}; edge agents the role of boundary authentication via EA_{ij} and manager agents the role of enforcing adjacency, survival and priority constraints; relaxations of m_{ij} to [0,1] permit convex surrogates and efficient rounding for large problems.

b) Decision-Making Process

Region, sub-region, and edge agents exploit prior knowledge from feature extraction to guide and improve task execution. Decision-making follows two complementary mechanisms.

- Mutual agreement convergence ensures agreement among agents observing the same data. A segmentation agent mediates the process, requiring majority support for a cooperation protocol, while minority agents conform to the group decision. The proposed Multi-Agent Merging Mutual Agreement Model adopts a delegation strategy based on homogeneity, similarity, and spatial proximity to enhance negotiation efficiency.

- Candidate selection identifies a refined set of alternatives from all agent proposals. This process comprises (i) a "fusion step", in which collective preferences are synthesized into a unified proposal, and (ii) an "exploitation step", where the selected proposal is executed.

4 Experimental results and discussion

Brain MRI segmentation methods face trade-offs in computational complexity and scalability for clinical application. Classical watershed methods are low-cost but suffer from over-segmentation and noise sensitivity. Machine learning and deep learning offer accuracy but require substantial resources and annotated datasets [50, 51, 52, 53], posing scalability challenges [54]. The WAMAS framework addresses this by integrating watershed segmentation with agent-based collaboration, enhancing scalability through decentralized control and adaptive decision-making for efficient processing of high-resolution MRI scans. Selecting the optimal detection method for specific benchmark datasets and noise models remains a critical challenge for comprehensive performance evaluation. Research increasingly focuses on adapting detection techniques to dataset characteristics and noise models to achieve high quantitative and qualitative metrics. Extracting relevant features from brain MRI images is essential due to complex tissue structures (white matter, gray matter, cerebrospinal fluid). MRI is used to determine tumor size and location, offering significant contrast differences among brain tissues compared to CT, PET, and SPECT [55]. MRI provides insights into tissue parameters such as proton density and relaxation times, facilitating precise brain tissue evaluation. T2-weighted MR images are frequently employed for pathological conditions, distinguishing tumor types and differentiating tumor from non-tumor tissues [56]. T1-weighted images with contrast enhancement delineate tumor boundaries [57]. Axial T2-weighted images with fluid-attenuated inversion recovery effectively visualize non-enhancing tumors, giving MRI a distinct advantage in brain tumor diagnosis [58]. This study aims to evaluate the efficiency, accuracy, robustness, and time-cost of the proposed WAMAS method using various benchmark datasets [59].

4.1 Test validation datasets

Validation tests typically require ground truth, which is often insufficient in clinical datasets, leading to subjective quality assessments. Proposed validation approaches include numerical data (synthetic or simulated) or physical phantoms with known features [60].

4.1.1 Numerical datasets

Numerical datasets, either synthetic or simulated, facilitate qualitative and quantitative evaluations due to their advantageous prior knowledge [61].

4.1.2 Synthetic datasets

Synthetic datasets may lack realistic anatomical or physical data, with or without added noise [62]. MRI simulators and simulated brain datasets are available from the McConnell Brain Imaging Centre [63].

4.1.3 Real datasets

The Internet Brain Segmentation Repository is an open-access resource providing MRI brain image data and validated segmentation results [64]. The Digital Imaging and Communications in Medicine dataset [65] was also used, despite lacking ground truth images [66].

4.2   Implementation framework

The WAMAS framework was implemented using C++, Pandora [67], and NetLogo programming languages in [68]. Python 3.6 was used for statistical visualizations. Tests were conducted on an Intel Core™ i7-3770K CPU (4GHz), 8GB RAM, and Windows 10 Professional. MRI brain images were sourced from a reputable medical image repository [63, 64, 65], and the algorithm's performance was compared against traditional methods.

4.3   Comparison of methods

The WAMAS framework for Brain MRI segmentation has been compared with KRFCMSC [69], a segmentation-based clustering algorithm particularly effective for MRI images [70]. KRFCMSC, in turn, was evaluated against five widely used clustering-based segmentation algorithms:

1. Fuzzy C-means (FCM) [71];

2. Rough Fuzzy C-means (RFCM) [72, 73];

3. Fuzzy   C-means   with   Spatial   Constraints (FCMSC) [74];

4. Kernelized Rough Fuzzy C-means (KRFCM) [75, 76];

5. Kernel Spatial Shadow C-means (KSSCM) [77].

In addition to these clustering-based approaches, WA-MAS was also compared with "state-of-the-art deep learning methods", namely U-Net and B-UNet [78], which represent the recent research direction in medical image segmentation.

This dual comparison is motivated by two main reasons:

- **Clustering-based methods** rely on "cluster merging strategies", which is conceptually close to the proposed "Watershed-based Variance Approach" in WAMAS, where segmentation is achieved through the merging of subregions based on variance. Thus, comparing with clustering methods highlights the improvements brought by WAMAS within the same family of merging-based techniques.

- **Deep learning-based methods** represent the "state-of-the-art axis of research", providing a strong baseline for evaluating the competitiveness of WAMAS against the most advanced approaches in medical image segmentation.

4.4   Validity indices utilized

The performance metrics calculated to quantitatively evaluate the quality of the segmentation proposed in this manuscript include Sensitivity (SA), Precision (Pr), Accuracy (Acc), and Recall. These metrics are summarized using the following formulas [79]:

Accuracy $= \frac{TP+TN}{TP+FP+FN+TN}$, Sensitivity (SA) $= \frac{TP}{TP+FN}$, Specificity $= \frac{TN}{TN+FP}$, Precision (Pr) $= \frac{TP}{TP+FP}$, Recall $= \frac{TP}{TP+FN}$, and Dice $= \frac{2TP}{2TP+FP+FN}$.

4.5   Tests and analysis

Table 2 demonstrates WAMAS's consistent superiority over classical segmentation methods across all tested datasets. Traditional approaches show high noise sensitivity and over-segmentation. WAMAS employs an agent-driven dynamic merging strategy guided by statistical variance, transforming over-segmented outputs into coherent regions and addressing a critical limitation of Watershed-based techniques.

WAMAS achieved 96.84% accuracy and 0.965 precision on IBSR18, outperforming Canny and Watershed. In Brain-Web, WAMAS consistently exceeded 92% accuracy, while conventional methods rarely surpassed 65%. These improvements, validated against radiologist-provided ground truth, confirm WAMAS's robustness in healthy and tumor-affected brain MRI. High sensitivity and Dice scores indicate precise pathological tissue detection, reducing false negatives. WAMAS maintains linear-to-quadratic computational complexity, ensuring scalable and accurate segmentation. Although edge cues may limit performance on ambiguous boundaries, WAMAS is a robust and accurate framework, promising for clinical decision support systems.

Table 3 highlights the superior robustness and generalizability of the proposed WAMAS framework compared with state-of-the-art deep learning models. While U-Net and its improved variant B-UNet [78] achieve strong performance on white matter (0.92) and gray matter (0.92–0.93), both exhibit noticeable degradation when segmenting cerebrospinal fluid (0.77–0.78), leading to a lower overall average (0.87–0.88). In contrast, WAMAS achieves consistently higher scores across all tissue classes, with 0.956 for white matter, 0.948 for gray matter, and 0.927 for cerebrospinal fluid, resulting in an average of 0.944.

This balanced improvement demonstrates that WAMAS not only excels in segmenting well-defined structures (WM, GM) but also handles the more challenging, low-contrast CSF regions with greater reliability, thereby reducing class-specific bias. The uniform performance across tissues indicates stronger generalizability to heterogeneous brain structures and pathologies, where conventional learning-based models often struggle due to training data limitations. Furthermore, unlike deep neural networks, which require extensive annotated datasets and retraining for new imaging modalities, WAMAS maintains its adaptability through its agent-driven dynamic merging mechanism, making it less dependent on domain-specific priors.

Empirical findings provide that WAMAS complements and potentially outperforms purely learning-based frameworks in both information (region and contour), particularly in tested samples where balanced empirical accuracy across multiple tissues is critical for diagnostic reliability (see Table 4).

A rigorous experimental design ensured consistency and reproducibility. WAMAS was evaluated on IBSR18 and BrainWeb datasets using multi-sequence 3T MRI images

Table 2: Average value of different performance metrics providing the efficiency of the proposed approach WAMAS using brain MRI images test sets from BrainWeb and IBSR datasets.

Datasets	Methods	SA	PR	ACC	Recall
IBSR167	Deriche	49.954	0.541	46.816	0.478
	Shen-Castan	46.514	0.443	42.847	0.371
	Canny	57.631	0.532	56.717	0.536
	Quadtree	39.172	0.347	45.214	0.416
	Watershed	15.204	0.079	11.541	0.073
	WAMAS	**92.517**	**0.915**	**90.967**	**0.905**
IBSR18	Deriche	46.991	0.497	44.533	0.481
	Shen-Castan	42.128	0.438	42.225	0.441
	Canny	63.312	0.596	58.423	0.548
	Quadtree	36.627	0.292	38.569	0.289
	Watershed	12.432	0.416	10.628	0.095
	WAMASA	**97.379**	**0.965**	**96.842**	**0.959**
BrainWeb (plane Z=85)	Deriche	52.663	0.326	26.041	0.096
	Shen-Castan	41.891	0.019	19.450	0.059
	Canny	65.334	0.510	28.498	0.062
	Quadtree	28.925	0.399	26.249	0.023
	Watershed	17.498	0.073	8.239	0.071
	WAMAS	**93.864**	**0.901**	**92.778**	**0.929**
BrainWeb (plane Z=100)	Deriche	54.516	0.483	52.446	0.518
	Shen-Castan	49.323	0.506	47.948	0.520
	Canny	67.604	0.618	66.539	0.624
	Quadtree	39.956	0.114	34.268	0.123
	Watershed	18.647	0.308	16.641	0.245
	WAMAS	**95.285**	**0.926**	**96.131**	**0.915**

Table 3: Comparative segmentation results on IBSR18: WAMAS versus state-of-the-art methods in [78]

Methods	WM	GM	CSF	Average
U-Net	0.920	0.920	0.770	0.870
B-UNet	0.930	0.920	0.780	0.880
WAMAS	**0.956**	**0.948**	**0.927**	**0.944**

(T1-weighted). Six representative subjects (three from IBSR18, three from BrainWeb) were randomly selected to test normal and tumor-affected brains. Experiments were repeated five times with different initializations; reported metrics are averaged scores with variances, ensuring statistical validation. Segmentation performance was assessed against radiologist-provided ground truth using accuracy, sensitivity, precision, and Dice coefficient. WAMAS consistently achieved superior results, including a peak accuracy of 97.38% on IBSR18 and balanced improvements across WM, GM, and CSF, outperforming U-Net and B-U-Net. Confidence intervals confirmed framework stability and mitigated dataset bias or noise sensitivity. IBSR18 was chosen for higher resolution, BrainWeb for synthetic variations. Correction routines minimized misalignments. Parameter selection was controlled (noise parameter fixed at 0.05), and multiple axial slices were evaluated to avoid overfitting.
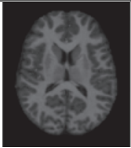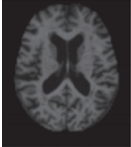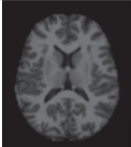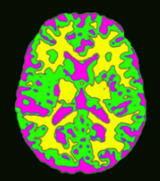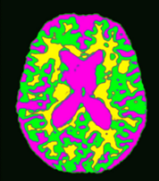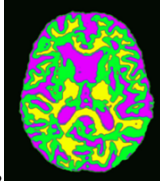
However, utilizing DICOM dataset images presents a significant challenge due to the lack of ground truth needed to confirm the accuracy of the proposed region-based MAS cooperation protocol, which relies heavily on the Watershed Merging style.

A robust stopping criterion was incorporated into the merging process for stability and reproducibility. Variance is iteratively computed between sub-regions and their parent regions as a statistical test. Merging halts if the criterion is not satisfied, preventing over-fusion and preserving critical tissue boundaries. This adaptive mechanism ensures convergence only when structural homogeneity is achieved. The criterion's robustness is validated both visually and quantitatively, showing higher accuracy and boundary precision than clustering-based methods. Figure 5 presents Box-and-Whisker plots from over 20 simulations on IBSR and BrainWeb, demonstrating narrow variance ranges. WAMAS achieved a mean accuracy of 93.97% with a variance of 5.12 across Z85, Z100, IBSR144, and IBSR150, yielding a 95% CI of 90.37–97.57%, confirming stable performance. These statistical results confirm the proposed stop condition is theoretically sound and empirically reliable, reinforcing WAMAS's superior consistency over conventional segmentation algorithms.

While conventional Watershed segmentation is prone to over-segmentation due to noise sensitivity, the proposed Watershed approach was rigorously tested for robustness. Test experiments were conducted on synthetic binary im-

Table 4: Simulated T1-wighted MR image from BrainWeb where z=50

ages contaminated with Rician (σ = 0.05) and "salt and pepper" noise (σ = 0.06) within brain MRI data. Permutation tests compared different clustering-based algorithms, including Fuzzy C-Means in the paper study based Kernelized Rough Fuzzy C-Means. The current method consistently exhibited higher average mean Dice values compared to other methods (Figure 6).

A consistent observation across permutation tests is that the ranking of segmentation methods remains stable when ordered by mean Recall values, not only across two distinct datasets (BrainWeb and IBSR) but also across multiple z-axis slices and IBSR dataset versions. This demonstrates that the proposed WAMAS framework generalizes beyond a single test configuration. Plots in (Figure 7) illustrate its consistent ability to delineate brain tissues under heterogeneous conditions, corroborated by the robustness of both Dice and Recall metrics. Specifically, WAMAS achieved Recall values ranging from 0.941 to 0.974 ($\pm$ 0.012, 95% CI [0.938–0.976]) across five BrainWeb slices (Z=55–100) and from 0.949 to 0.971 ($\pm$ 0.010, 95% CI:[0.947–0.972]) across multiple IBSR versions (IBSR144–IBSR18). In contrast, KRFCMSC fluctuated between 0.807–0.909 ($\pm$0.035) and FCM between 0.658–0.721 ($\pm$0.026). The narrow variance ranges and tight confidence intervals confirm WAMAS's reproducibility and adaptability, underscoring its ability to generalize segmentation accuracy under diverse acquisition settings and anatomical structures.

The proposed WAMAS framework for brain MRI seg-

mentation employs an iterative bottom-up strategy in which agents are assigned to sub-regions and progressively merged until convergence. Convergence is reached when the variance between two merging clusters across consecutive iterations falls below a threshold of 0.001, signifying that no further meaningful changes occur. Figure 8 illustrates this process for representative IBSR and Brain-Web datasets, showing that the disparity between merging clusters decreases steadily until stability is achieved. This behavior confirms that WAMAS converges reliably while producing anatomically consistent tissue boundaries.

Performance differences compared to classical methods are explained by WAMAS's dynamic, variance-driven merging. Unlike Watershed, which produces excessive fragmented regions, or noise-sensitive edge detectors, WAMAS adaptively consolidates sub-regions into coherent structures, improving Dice similarity and Recall. The number of agents is critical for balancing segmentation quality and computational cost. Empirical results show 50 agents risk under-segmentation, 100 agents offer an optimal trade-off, and 200 agents provide marginal precision improvement at double the convergence time. WAMAS achieves robustness and generalizability by maintaining stability across datasets with a practical number of agents for efficiency and accuracy.

WAMAS achieves low computational complexity primarily due to its parallel agent-based design. Independent agents assigned to sub-regions distribute the segmentation process across multiple CPU threads, significantly
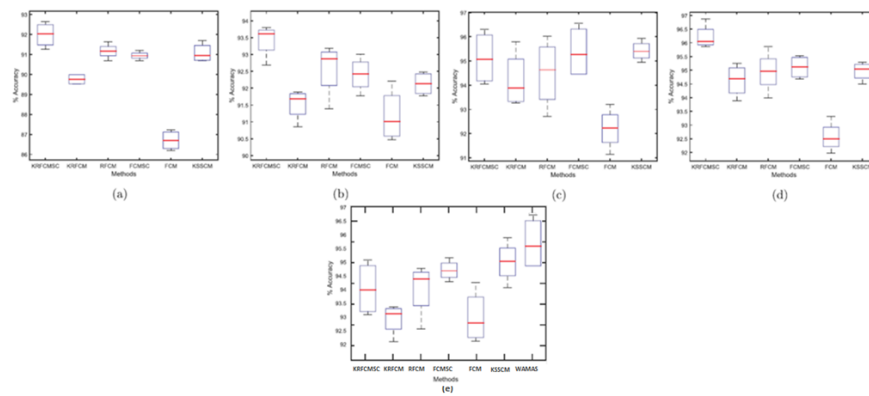
Figure 5: Boxplots of average segmentation accuracies (%) from 10 Simulations on BrainWeb (z=85, 5% rician noise) comparing WAMAS with state of the art methods in [69].
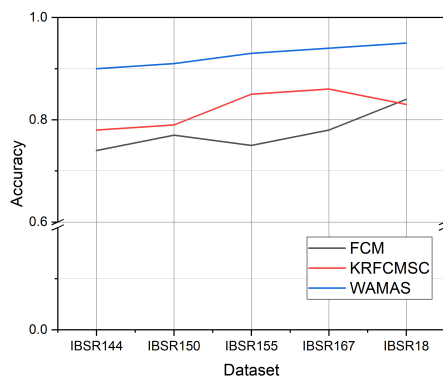

Figure 6: Quantitative comparison using dice coefficient metrics for FCM, KRFCMSC cited in [69], and the proposed WAMAS using BrainWeb MRI data.

Figure 7: Quantitative analysis of recall scores from (a) FCM/KRFCMSC [69] and (b) WAMAS on BrainWeb datasets (Z=55–100).

Figure 8: Convergence of the proposed merging process across four datasets: IBSR 167, IBSR 18, BrainWeb (z=85), and BrainWeb (Z=100).

reducing runtime and ensuring scalability. The most intensive step, iterative variance calculation, is localized within each agent's sub-region and amortized by the parallel architecture. Most WAMAS tasks operate at linear $O_{(\eta)}$ or quadratic $O_{(\eta^2)}$ time. Thanks to synchronization and constraints, variance computation does not become a bottleneck. The design balances lightweight intensity-based features and synchronized agent cooperation for low memory and runtime, with variance-based merging guaranteeing precision and robustness.

In terms of scalability, "WAMAS demonstrates a clear computational advantage". Operating directly on 2D image structures, it is seamlessly applicable to diverse datasets without modification, ensuring broad usability and eliminating dataset-specific tuning (Figure 9).

Furthermore, WAMAS segments images into multiple regions simultaneously, reducing overall processing time. This multi-region capability, illustrated in Figure 10, directly lowers computational overhead in large-scale segmentation. The agent-based design inherently supports "parallel execution"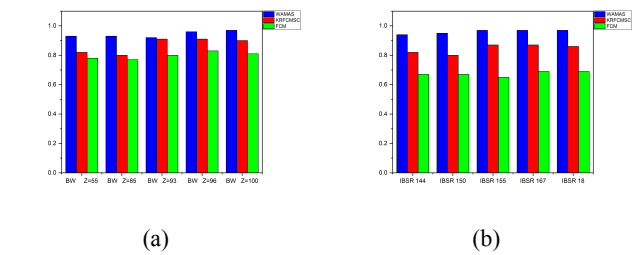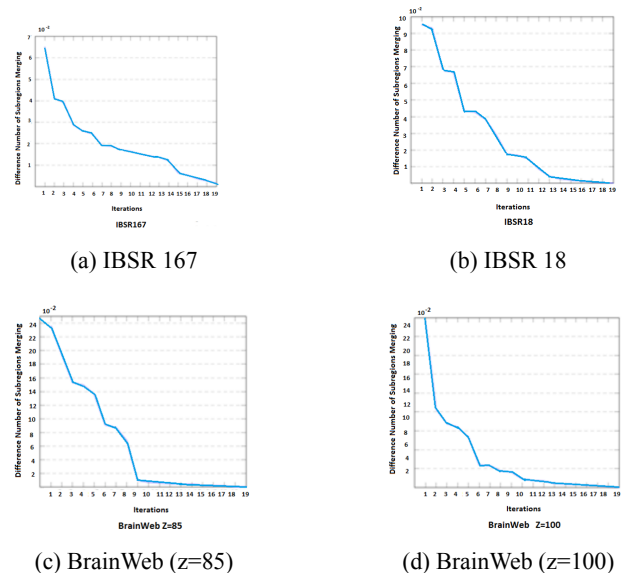 on multiple CPU cores, distributing computations across threads to accelerate processing for large image sets without sacrificing accuracy.

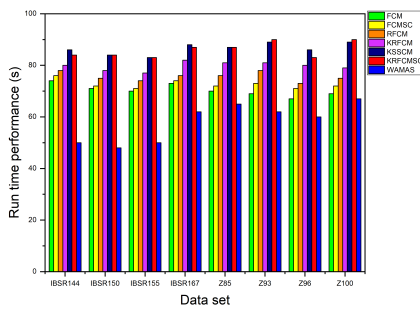Equally critical is "memory efficiency". Since agents

Figure 9: Runtime performance (in seconds) of WAMAS vs. KRFCMSC, FCM, FCMSC, RFCM, and KRFCM based on [69].
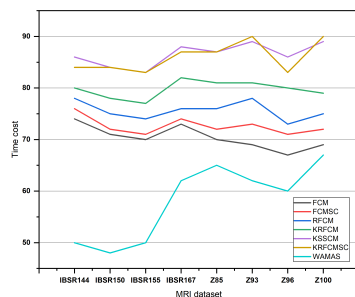

Figure 10: Time-cost evaluation of the proposed WAMAS framework compared with approaches cited in [69].

process only local information and exchange lightweight statistical measures, the framework minimizes storage requirements and avoids costly global computations. This decentralized memory usage ensures that WAMAS remains practical even for high-resolution images or large-scale datasets, where conventional segmentation methods often face bottlenecks.

From a computational standpoint : - the overall complexity of WAMAS scales near-linearly with the number of image pixels (O_η), while parallelism across agents further reduces effective runtime. This ensures that performance degrades gracefully as image size increases, establishing WAMAS as a scalable, memory-efficient, and computationally robust framework for diverse and high-volume image segmentation scenarios.

- the proposed WAMAS framework consistently outperforms conventional watershed methods, achieving efficient execution times across multiple datasets and versions.

- its cooperative agent-based design enhances scalability, enabling parallel execution on multi-core CPUs while maintaining high recall and accuracy in Brain MRI segmentation.

- WAMAS significantly reduces over-segmentation by merging region seeds more effectively, leading to cleaner and more distinct partitions.

- The novelty lies in integrating watershed locally within regions while leveraging MAS-driven dynamic merging and distributed processing to address noise sensitivity and indistinct boundaries.

5 Conclusion

Early detection of brain cancer is the key to raise the success of diagnostic rate of treatment. In this context, MRI remains the predominant imaging modality for screening. However, the segmentation of MRI images for brain cancer detection presents significant challenges due to the inherent ambiguity and overlapping nature of brain structures. Moreover, noisy MRIs, often caused by radiofrequency coils, exacerbate the difficulty of image segmentation. These noisy images contain high-frequency content in edge, region, and noise components, resulting in fragmented outlines and potential misidentification of tumor locations.

To address these challenges, a segmentation framework based on a Multi-Agent System (MAS) emerges as a crucial tool for achieving satisfactory segmentation outcomes. This framework allows users to create distributed systems comprising interacting agents within an environment, enabling perception and action. The parallelism inherent in this approach significantly reduces the time-cost, as each operation (such as edge and region detection) can be executed independently.

In particular, this work contributes to the field by introducing a bottom-up approach within the Watershed technique, incorporating a set of constraints and a "Dynamic Merging style" with "stop criteria". These enhancements facilitate algorithm convergence, leading to improved segmentation results.

Crucially, the proposed approach focuses on the interaction among agents and how they communicate to facilitate the detection of relevant objects. This is achieved through well-defined priorities that support a rational decision-making process. Agents play a pivotal role in achieving accurate segmentation by following specific interaction protocols that break down the complex problem into subproblems, ultimately leading to effective problem-solving.

This approach successfully separates regions in space, accurately segmenting regions with similar properties. Comparative analysis with other methods discussed in the results section demonstrates significant improvements in the obtained results.

As perspective, future research will explore postprocessing techniques to enhance the accuracy of the current work. This includes de-noising MRI images resulting from the segmentation process. Additionally, the framework can utilize an edge-map generated within the framework, define markers for all edges, and employ agent-based inference to select the most suitable combination of feature extraction techniques. These endeavors aim to further advance the accuracy and robustness of the segmentation process.

References

[1] Argunçsah, Ali Özgür, Ertunc Erdil, and Devrim Ünay. "Applications of Computer Vision and Machine Learning in Bioimaging." In *Bioimaging Modalities in Bioengineering*, pp. 585–626. Springer, 2025.

[2] Çukur, Tolga, Salman UH Dar, Valiyeh Ansarian Nezhad, Yohan Jun, Tae Hyung Kim, Shohei Fujita, and Berkin Bilgic. "A tutorial on MRI reconstruction: From modern methods to clinical implications." *arXiv preprint arXiv:2507.16715*, 2025.
`https://doi.org/10.1109/TBME.2025.`
`3617575`

[3] Cobbinah, Matthew, Henry Nunoo-Mensah, Prince Ebenezer Adjei, Francisca Adoma Acheampong, Isaac Acquah, Eric Tutu Tchao, Andrew Selasi Agbemenu, Jerry John Kponyo, and Emmanuel Abaidoo. "Diversity in Stable GANs: A Systematic Review of Mode Collapse Mitigation Strategies." *Engineering Reports* 7, no. 6 (2025): e70209.
`https://doi.org/10.1002/eng2.70209`

[4] Jin, Chengcheng, Theam Foo Ng, and Haidi Ibrahim. "Advancements in Semi-Supervised Deep Learning for Brain Tumor Segmentation in MRI: A Literature Review." *AI* 6, no. 7 (2025): 153.
`https://doi.org/10.3390/ai6070153`

[5] Tae, Woo-Suk, Byung-Joo Ham, Sung-Bom Pyun, and Byung-Jo Kim. "Current Clinical Applications of Structural MRI in Neurological Disorders." *Journal of Clinical Neurology (Seoul, Korea)* 21, no. 4 (2025): 277.
`https://doi.org/10.3988/jcn.2025.0185`

[6] Rong, Yi, Riley Tegtmeier, Edward L. Clouser Jr, Sujay A. Vora, Chang-Shiun Lin, Thomas R. Mackie, Robert Timmerman, and Mu-Han Lin. "Advancements in radiation therapy treatment workflows for precision medicine: a review and forward looking." *International Journal of Radiation Oncology*Biology*Physics* 122, no. 4 (2025): 1022–1034.
`https://doi.org/10.1016/j.ijrobp.2025.`
`04.010`

[7] Sujji, G. Evelin, YVS Lakshmi, and G. Wiselin Jiji. "MRI brain image segmentation based on thresholding." *International Journal of Advanced Computer Research* 3, no. 1 (2013): 97.

[8] Hsieh, Thomas M., Yi-Min Liu, Chun-Chih Liao, Furen Xiao, I-Jen Chiang, and Jau-Min Wong. "Automatic segmentation of meningioma from non-contrasted brain MRI integrating fuzzy clustering and region growing." *BMC Medical Informatics and Decision Making* 11, no. 1 (2011): 54.
`https://doi.org/10.1186/1472-6947-11-54`

[9] Silvoster, M. Leena, R. Mathusoothana, and S. Kumar. "Watershed based algorithms for the segmentation of spine MRI." *International Journal of Information Technology* 14, no. 3 (2022): 1343–1353.
`https://doi.org/10.1007/`
`s41870-021-00644-8`

[10] Vadmal, Vachan, Grant Junno, Chaitra Badve, William Huang, Kristin A. Waite, and Jill S. Barnholtz-Sloan. "MRI image analysis methods and applications: an algorithmic perspective using brain tumors as an exemplar." *Neuro-Oncology Advances* 2, no. 1 (2020): vdaa049.
`https://doi.org/10.1093/noa/vdaa049`

[11] Xu, Yan, Rixiang Quan, Weiting Xu, Yi Huang, Xiaolong Chen, and Fengyuan Liu. "Advances in medical image segmentation: A comprehensive review of traditional, deep learning and hybrid approaches." *Bioengineering* 11, no. 10 (2024): 1034.
`https://doi.org/10.3390/`
`bioengineering11101034`

[12] Xiao, Yating, Yan Chen, Yong Zhang, Runjie Zhang, Guangyu Cui, Yufeng Song, and Quan Zhang. "Spine X-ray image segmentation based on deep learning and marker controlled watershed." *Journal of X-Ray Science and Technology* 33, no. 1 (2025): 109–119.
`https://doi.org/10.3233/XST-240100`

[13] Aelgani, Vivekanand, Suneet Kumar Gupta, and V. A. Narayana. "A 2-level meta-heuristic aware adaptive watershed technique based optimized convolutional deep neural network for lung cancer segmentation and classification using explainable AI." *Biomedical Signal Processing and Control* 103 (2025): 107395.
`https://doi.org/10.1016/j.bspc.2024.`
`107395`

[14] Abinav, S. "Automated segmentation and classification of soft tissues in pathology images using deep learning and improved watershed algorithms." [Unpublished manuscript].

[15] Krishnapriya, Srigiri, and Yepuganti Karuna. "A survey of deep learning for MRI brain tumor segmentation methods: Trends, challenges, and future directions." *Health and Technology* 13, no. 2 (2023): 181–201.
`https://doi.org/10.1007/`
`s12553-023-00737-3`

[16] Latha, C., and K. Perumal. "Suppression of Over-Segmentation in Watershed Segmentation." *International Journal of Computer Science and Information Security (IJCSIS)* 14, no. 10 (2016).

[17] Lee, Jeong-A, et al. "Automated Brain Image Segmentation from Magnetic Resonance Image Using

SVM and Watershed Transform." PhD diss., Chosun University, 2020.

[18] Yeghiazaryan, Varduhi, Yeva Gabrielyan, and Irina Voiculescu. "Parallel Watershed Partitioning: GPU-Based Hierarchical Image Segmentation." *Journal of Parallel and Distributed Computing* (2025): 105140. https://doi.org/10.1016/j.jpdc.2025.105140

[19] Do, Thanh-Ha, Hoang Minh-Huong Dang, Thanh-Lam Tran, Van-De Nguyen, et al. "Two-stage Pipeline for Automated Cell Segmentation: Integrating Semantic and Instance Learning." *APSIPA Transactions on Signal and Information Processing* 14, no. 1 (2025). https://doi.org/10.1561/116.20250033

[20] Golkarieh, Alireza, Sajjad Rezvani Boroujeni, Kiana Kiashemshaki, Maryam Deldadehasl, Hamed Aghayarzadeh, and Azita Ramezani. "Breakthroughs in brain tumor detection: leveraging deep learning and transfer learning for MRI-based classification." *Computer and Decision Making: An International Journal* 2 (2025): 708–722.

[21] Musthafa, Namya, Qurban A. Memon, and Mohammad M. Masud. "Advancing Brain Tumor Analysis: Current Trends, Key Challenges, and Perspectives in Deep Learning-Based Brain MRI Tumor Diagnosis." *Eng* 6, no. 5 (2025): 82. https://doi.org/10.3390/eng6050082

[22] Birjais, Roshan. "Challenges and Future Directions for Segmentation of Medical Images Using Deep Learning Models." In *Deep Learning Applications in Medical Image Segmentation: Overview, Approaches, and Challenges*, pp. 243–264. Wiley, 2025. https://doi.org/10.1002/9781394245369.ch11

[23] Rasool, Novsheena, and Javaid Iqbal Bhat. "A critical review on segmentation of glioma brain tumor and prediction of overall survival." *Archives of Computational Methods in Engineering* 32, no. 3 (2025): 1525–1569. https://doi.org/10.1007/s11831-024-10188-2

[24] Mankki, Jussi-Jaakko, and Klavdiia Bochenina. "Vision Transformers in Brain Image Segmentation." University of Helsinki, 2025.

[25] Wei, Yujia, Jaidip Manikrao Jagtap, Yashbir Singh, Bardia Khosravi, Jason Cai, Jeffrey L. Gunter, and Bradley J. Erickson. "Comprehensive Segmentation of Gray Matter Structures on T1-Weighted Brain MRI: A Comparative Study of CNN, CNN Hybrid-Transformer or Mamba Architectures." *American Journal of Neuroradiology* 46, no. 4 (2025): 742–749. https://doi.org/10.3174/ajnr.A8544

[26] Dihin, Rasha Ali, and Nesreen Readh Hamza. "Brain Tumor Classification in MRI Images Using VGG19 with Type2 Fuzzy Logic." *Informatica* 49, no. 13 (2025). https://doi.org/10.31449/inf.v49i13.7161

[27] Raghuramaiah, Bandla, and Suresh Chittineni. "BreastEnsemNet: Transformer and BiLSTM-Based Hybrid Ensemble Deep Learning for Mammogram Classification." *Informatica* 49, no. 31 (2025). https://doi.org/10.31449/inf.v49i31.8501

[28] Lu, Yuting, et al. "An improved watershed segmentation algorithm of medical tumor image." IOP Conference Series: Materials Science and Engineering. Vol. 677. No. 4. IOP Publishing, 2019. https://doi.org/10.1088/1757-899X/677/4/042028

[29] Kornilov, Anton, Ilia Safonov, and Ivan Yakimchuk. "A review of watershed implementations for segmentation of volumetric images." Journal of Imaging 8.5 (2022): 127. https://doi.org/10.3390/jimaging8050127

[30] Roy, Bijoyeta, Mousumi Gupta, and Bidyut Krishna Goswami. "Revolutionizing colon histopathology glandular segmentation using an ensemble network with watershed algorithm." International Journal of Imaging Systems and Technology 34.5 (2024): e23179. https://doi.org/10.1002/ima.23179

[31] Xiao, Yating, et al. "Spine X-ray image segmentation based on deep learning and marker controlled watershed." Journal of X-Ray Science and Technology 33.1 (2025): 109-119. https://doi.org/10.3233/XST-240100

[32] Annavarapu, Ambika, and Surekha Borra. "An adaptive watershed segmentation based medical image denoising using deep convolutional neural networks." Biomedical Signal Processing and Control 93 (2024): 106119. https://doi.org/10.1016/j.bspc.2024.106119

[33] Shen, Xiaoyan, et al. "Lesion segmentation in breast ultrasound images using the optimized marked watershed method." Biomedical Engineering Online 20.1 (2021): 57. https://doi.org/10.1186/s12938-021-00891-7

[34] Guo, Miao, Ating Yang, and Min Dong. "Breast Mass Segmentation via Enhanced U-Net++ Using Gradient and Contrast Information Reconstruction." Informatica 49.25 (2025). https://doi.org/10.31449/inf.v49i25.8483

[35] Xu, Qi. "Adaptive Semantic Perception Model for Deep Learning-Based Image Processing and Pattern Recognition." Informatica 49.29 (2025). `https://doi.org/10.31449/inf.v49i29.8724`

[36] Mezzoudj, Saliha, Meriem Khelifa, and Yasmina Saadna. "Leveraging Spark-TensorFlow Distributor for Distributed Deep Convolutional Neural Networks: Accelerating large-scale COVID-19 Detection." Informatica 49.17 (2025). `https://doi.org/10.31449/inf.v49i17.7505`

[37] Tiwary, Pradeep Kumar, Prashant Johri, Alok Katiyar, and Mayur Kumar Chhipa. "Deep Learning-Based MRI Brain Tumor Segmentation with EfficientNet-Enhanced UNet." IEEE Access (2025). `https://doi.org/10.1109/ACCESS.2025.10938151`

[38] Tejashwini, P. S., J. Thriveni, and K. R. Venugopal. "A novel SLCA-UNet architecture for automatic MRI brain tumor segmentation." Biomedical Signal Processing and Control 100 (2025): 107047. `https://doi.org/10.1016/j.bspc.2024.107047`

[39] Bhatti, Uzair Aslam, Jinru Liu, Mengxing Huang, and Yu Zhang. "FF-UNet: Feature fusion based deep learning-powered enhanced framework for accurate brain tumor segmentation in MRI images." Image and Vision Computing (2025): 105635. `https://doi.org/10.1016/j.imavis.2025.105635`

[40] Khaleel, Zahraa, and Amir Lakizadeh. "Early Diagnosis of Alzheimer's Disease with Transfer Learning Techniques Via ResNet50 and FSBi-LSTM." Informatica 49.11 (2025). `https://doi.org/10.31449/inf.v49i11.7352`

[41] Saifullah, Shoffan, Rafał Dreżewski, Anton Yudhana, Maciej Wielgosz, and Wahyu Caesarendra. "Modified U-Net with attention gate for enhanced automated brain tumor segmentation." Neural Computing and Applications 37.7 (2025): 5521–5558. `https://doi.org/10.1007/s00521-024-10919-3`

[42] Ho, Hsing-Hao, Huai-Che Yang, Wen-Xiang Yang, Cheng-Chia Lee, Hsiu-Mei Wu, I-Chun Lai, Ching-Jen Chen, and Syu-Jyun Peng. "Deep learning for automated segmentation of radiation-induced changes in cerebral arteriovenous malformations following radiosurgery." BMC Medical Imaging 25.1 (2025): 218. `https://doi.org/10.1186/s12880-025-01796-w`

[43] Angona, Tazkia Mim, and M. Rubaiyat Hossain Mondal. "An attention based residual U-Net with swin transformer for brain MRI segmentation." Array 25 (2025): 100376. `https://doi.org/10.1016/j.array.2025.100376`

[44] Allioui, Hanane, Mohamed Sadgal, and Aziz Elfazziki. "Intelligent environment for advanced brain imaging: multi-agent system for an automated Alzheimer diagnosis." Evolutionary Intelligence 14.4 (2021): 1523-1538. `https://doi.org/10.1007/s12065-020-00420-w`

[45] Bennai, Mohamed Tahar, Zahia Guessoum, Smaine Mazouzi, Stephane Cormier, and Mohamed Mezghiche. "A Stochastic Multi-Agent Approach for Medical-Image Segmentation: Application to Tumor Segmentation in Brain MR Images." Artificial Intelligence in Medicine 110 (2020): 101980. `https://doi.org/10.1016/j.artmed.2020.101980`

[46] Xia, Zhaoyue, Jun Du, Jingjing Wang, Chunxiao Jiang, Yong Ren, Gang Li, and Zhu Han. "Multi-Agent Reinforcement Learning Aided Intelligent UAV Swarm for Target Tracking." IEEE Transactions on Vehicular Technology PP (2021): 1–1. `https://doi.org/10.1109/TVT.2021.3129504`

[47] Elkamouchi, Rahma, Abdelaziz Daaif, and Kamal Elguemmat. "Multi-Agents System in Healthcare: A Systematic Literature Review." International Conference on Smart Applications and Data Analysis. Cham: Springer Nature Switzerland, 2024. `https://doi.org/10.1007/978-3-031-77043-2_15`

[48] Montagna, Sara, et al. "Agent-based systems in healthcare." Computer Methods and Programs in Biomedicine 248 (2024): 108140. `https://doi.org/10.1016/j.cmpb.2024.108140`

[49] Bennai, Mohamed T., et al. "Multi-agent medical image segmentation: A survey." Computer Methods and Programs in Biomedicine 232 (2023): 107444. `https://doi.org/10.1016/j.cmpb.2023.107444`

[50] Radiopaedia. "Watershed cerebral infarction." Available at: `https://radiopaedia.org/articles/watershed-cerebral-infarcmtion`

[51] Cufi, X., Munoz, X., Freixenet, J., Marti, J. "A review of image segmentation techniques integrating region and boundary information." Advances in Imaging and Electron Physics, 120, pp. 1–39, 2003, Elsevier. `https://doi.org/10.1016/S1076-5670(02)80033-7`

[52] Karma, I. G. M., Putra, I. K. G. D., Sudarma, M., Linawati, L. "Image Segmentation Based on Color Dissimilarity." Informatica, vol. 46, no. 5, 2022. `https://doi.org/10.31449/inf.v46i5.3645`

[53] Jasim, H. M., Ghrabat, M. J. J., Abdulrahman, L. Q., Nyangaresi, V. O., Ma, J., Abduljabbar, Z. A., Abduljaleel, I. Q. "Provably efficient multi-cancer image segmentation based on multi-class fuzzy entropy." Informatica, vol. 47, no. 8, 2023. `https://doi.org/10.31449/inf.v47i8.4840`

[54] Al-Kharaz, A. A. "Optimization of Brain Cancer Images with Some Noise Models." Informatica, vol. 47, no. 9, 2023. `https://doi.org/10.31449/inf.v47i9.4566`

[55] Rastogi, D., Johri, P., Donelli, M., Kadry, S., Khan, A. A., Espa, G., Feraco, P., Kim, J. "Deep learning-integrated MRI brain tumor analysis: feature extraction, segmentation, or Survival Prediction using Replicator and volumetric networks." Scientific Reports, vol. 15, no. 1, pp. 1437, 2025, Nature Publishing Group UK London. `https://doi.org/10.1038/s41598-024-84386-0`

[56] Möller, H., Graf, R., Schmitt, J., Keinert, B., Schön, H., Atad, M., Sekuboyina, A., Streckenbach, F., Kofler, F., Kroencke, T., et al. "SPINEPS—automatic whole spine segmentation of T2-weighted MR images using a two-phase approach to multi-class semantic and instance segmentation." European Radiology, vol. 35, no. 3, pp. 1178–1189, 2025, Springer. `https://doi.org/10.1007/s00330-024-11155-y`

[57] Aruna, V. S., Vijayashree, J. "A Critical Analysis of Brain Tumor MRI Segmentation and Classification Utilizing Machine Learning and Deep Learning Methods." Informatica, vol. 49, no. 24, 2025. `https://doi.org/10.31449/inf.v49i24.8202`

[58] Al-Fakih, Abdulkhalek, et al. "FLAIR MRI sequence synthesis using squeeze attention generative model for reliable brain tumor segmentation." *Alexandria Engineering Journal*, vol. 99, 2024, pp. 108–123. `https://doi.org/10.1016/j.aej.2024.04.068`

[59] Aljahdali, Sadeem, et al. "Effectiveness of radiology modalities in diagnosing and characterizing brain disorders." *Neurosciences Journal*, vol. 29, no. 1, 2024, pp. 37–43. `https://doi.org/10.17712/nsj.2024.1.202300067`

[60] Collins, D. L., A. P. Zijdenbos, V. Kollokian, J. G. Sled, N. J. Kabani, C. J. Holmes, et al. "Design and construction of a realistic digital brain phantom." *IEEE Transactions on Medical Imaging*, vol. 17, no. 3, 1998, pp. 463–468. `https://doi.org/10.1109/42.712135`

[61] Chatterjee, Pubali, Kaushik Das Sharma, and Amlan Chakrabarti. "A stochastic approach for automated brain MRI segmentation." *IET Image Processing*, vol. 15, no. 3, 2021, pp. 735–745. `https://doi.org/10.1049/ipr2.12058`

[62] Chen, Hsian-Min, et al. "Comparison of Multispectral Image-Processing Methods for Brain Tissue Classification in BrainWeb Synthetic Data and Real MR Images." *BioMed Research International*, vol. 2021, 2021, 9820145. `https://doi.org/10.1155/2021/9820145`

[63] BrainWeb dataset. Freely available at: `http://brainweb.bic.mni.mcgill.ca/brainweb/`

[64] IBSR dataset. Freely available at: `https://www.nitrc.org/projects/ibsr/`

[65] DICOM dataset. Freely available at: `https://www.osirix-viewer.com/resources/dicom-image-library/`

[66] Rutherford, M., Mun, S. K., Levine, B., Bennett, W., Smith, K., Farmer, P., Jarosz, Q., Wagner, U., Freyman, J., Blake, G., et al. "A DICOM dataset for evaluation of medical image de-identification." Scientific Data, vol. 8, no. 1, pp. 183, 2021, Nature Publishing Group UK London. `https://doi.org/10.1038/s41597-021-00967-y`

[67] Pandora: Agent-Based Modelling framework for large-scale distributed simulations. Freely available online at: `https://github.com/xrubio/pandora`

[68] Wilensky, Uri. *NetLogo Version 6.4.0* Center for Connected Learning and Computer-Based Modeling, Northwestern University, 2021. Available at: `https://ccl.northwestern.edu/netlogo`

[69] Halder, A., Talukdar, N. A. "Brain tissue segmentation using improved kernelized rough-fuzzy C-means with spatio-contextual information from MRI." Magnetic Resonance Imaging, vol. 62, pp. 129–151, 2019, Elsevier. `https://doi.org/10.1016/j.mri.2019.06.010`

[70] Hall, L. O., Bensaid, A. M., Clarke, L. P., Velthuizen, R. P., Silbiger, M. S., Bezdek, J. C. "A comparison of neural network and fuzzy clustering techniques in segmenting magnetic resonance images of the brain." IEEE Transactions on Neural Networks, vol. 3, no. 5, pp. 672–682, 1992, IEEE. `https://doi.org/10.1109/72.159057`

[71] Li, C., Goldgof, D. B., Hall, L. O. "Knowledge-based classification and tissue labeling of MR images of human brain." IEEE Transactions on Medical Imaging, vol. 12, no. 4, pp. 740–750, 1993, IEEE.
https://doi.org/10.1109/42.251125

[72] Maji, P., Pal, S. K. "Rough-fuzzy pattern recognition: applications in bioinformatics and medical imaging." John Wiley & Sons, 2012.
https://doi.org/10.1002/9781118112731

[73] Maji, P., Pal, S. K. "RFCM: a hybrid clustering algorithm using rough and fuzzy sets." Fundamenta Informaticae, vol. 80, no. 4, pp. 475–496, 2007, SAGE Publications Sage UK: London, England.
https://doi.org/10.3233/FI-2007-80408

[74] Ahmed, M. N., Yamany, S. M., Mohamed, N., Farag, A. A., Moriarty, T. "A modified fuzzy c-means algorithm for bias field estimation and segmentation of MRI data." IEEE Transactions on Medical Imaging, vol. 21, no. 3, pp. 193–199, 2002, IEEE.
https://doi.org/10.1109/42.996338

[75] Halder, A. "Kernel based rough fuzzy c-means clustering optimized using particle swarm optimization." In: 2015 International Symposium on Advanced Computing and Communication (ISACC), pp. 41–48, 2015, IEEE.
https://doi.org/10.1109/ISACC.2015.7377312

[76] Chen, S., Zhang, D. "Robust image segmentation using FCM with spatial constraints based on new kernel-induced distance measure." IEEE Transactions on Systems, Man, and Cybernetics, Part B (Cybernetics), vol. 34, no. 4, pp. 1907–1916, 2004, IEEE.
https://doi.org/10.1109/TSMCB.2004.831165

[77] Chen, L., Zou, J., Chen, C. L. P. "Kernel Spatial Shadowed C-Means for Image Segmentation." International Journal of Fuzzy Systems, vol. 16, no. 1, 2014

[78] Tavares, S. "White Matter, Gray Matter and Cerebrospinal Fluid Segmentation from Brain Magnetic Resonance Imaging using Adaptive U-Net and Local Convolutional Neural Network."

[79] Müller, D., Soto-Rey, I., Kramer, F. "Towards a guideline for evaluation metrics in medical image segmentation." BMC Research Notes, vol. 15, no. 1, pp. 210, 2022, Springer.
https://doi.org/10.1186/s13104-022-06096-y